



Hydrogen charging of carbon and low alloy steel by electrochemical methods

Fabio Bolzoni¹ · Luca Paterlini¹ · Luca Casanova¹ · Marco Ormellese¹

Received: 29 March 2023 / Accepted: 26 June 2023 / Published online: 4 July 2023
© The Author(s) 2023

Abstract

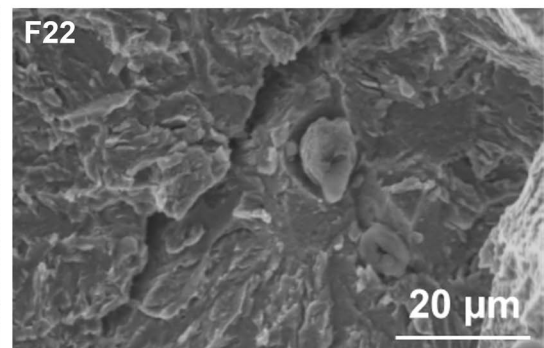
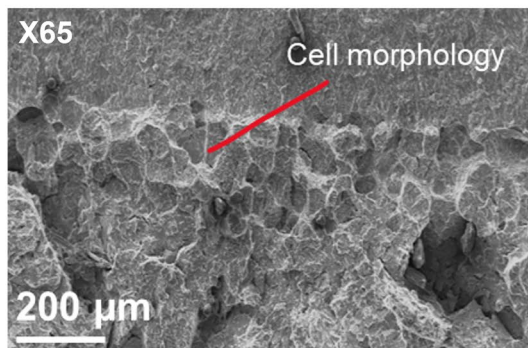
Atomic hydrogen can be the result of different processes like electroplating, chemical and electrochemical pickling treatments, in welding or by cathodic processes in corrosive fluids. Moreover, adsorption of atomic hydrogen can affect materials in contact with high pressure gaseous hydrogen. Once entered the material, atomic hydrogen interacts with the metal structure and may produce a “damage” of various forms, such as Hydrogen Induced Cracking (HIC), delayed fracture, blistering and hydrogen embrittlement. In particular, when H₂S is present (“sour service”), metallic materials, such as carbon and low alloy steels, may suffer hydrogen damage and hydrogen embrittlement. Sour service materials must be used in compliance with international accepted standards, used worldwide in oil and gas activities, when fluids are classified as sour. The present study has been carried out in order to set up an electrochemical method to charge with hydrogen two typical pipeline materials, carbon and low alloy steels. The reason of the use of an electrochemical method is to avoid any critical conditions from the point of view of preparation, safety and disposal. Hydrogen content in the specimens was measured by two different methods: hot glycerol bath and Inert Gas Fusion (IGF) analysis. Hydrogen content in the specimens is about 0.6–2 ppm; mechanical performances were assessed by means of J integral tests: a pronounced decrease of fracture toughness was observed for H charged specimens.

Graphical Abstract

H charging of CT samples



Fracture morphology of H charged metals after J integral test



Keywords Hydrogen embrittlement (HE) · Electrochemical charging · H₂S · Hydrogen gas

✉ Luca Casanova
luca.casanova@polimi.it

¹ Department of Chemistry, Materials and Chemical Engineering “G. Natta”, Politecnico di Milano, Via Mancinelli 7, 20131 Milano, Italy

1 Introduction

Atomic hydrogen can be the result of processes very different in nature like electroplating (chrome plating, galvanizing and phosphating), chemical and electrochemical pickling treatments, in welding if the humidity of consumables is too high,

or by cathodic processes developing in corrosive fluids: in this last case, so called cathodic poisoners, as H_2S , can inhibit molecular hydrogen formation promoting atomic hydrogen adsorption and diffusion into the metal. In atmospheres containing gaseous hydrogen once the molecular orbital of H_2 interact with the Fermi level of the metal a chemical dissociation of the molecule occurs and eventually atomic H may be absorbed inside the hosting structure. The content of absorbed H is generally a function of the surface fugacity which is seen to be proportional, in case of ferritic steels, to the square root of the gas pressure according to the Sieverts law [1].

Once entered the material, atomic hydrogen interacts with the metal structure and may produce a “damage” of various forms, such as HIC (hydrogen induced cracking), delayed fracture, blistering and hydrogen embrittlement [2–4]. Several theories have been proposed even if none of them was able to describe the phenomenon completely [5].

H embrittlement can be evaluated according to several mechanical tests belonging to fracture mechanics like J-integral, evaluating the decrease of toughness experienced by H charged metals, or fatigue tests, where H presence particularly affects the propagation stages of the crack growth.

Carbon and low alloy steels are commonly used in Oil and Gas industry when generalized corrosion due to the presence of CO_2 and H_2S is considered acceptable to stand the design life. However, when sour condition applies, the occurrence of Sulphide Stress Corrosion Cracking (SSCC) in the presence of H_2S on susceptible materials must be investigated [6, 7].

The goal of the paper is to find a procedure for the electrochemical charging in order to simulate the conditions occurring in pipeline steels affected by the entry of atomic hydrogen. The reason of the use of an electrochemical method is to avoid any critical conditions from the point of view of preparation, safety and disposal, as in the case of charging in solution with H_2S or gaseous hydrogen.

Two very “clean” pipeline steels (one carbon steel and one low alloy steel), produced through a normal commercial production line, were used for the experimental tests. Electrochemical hydrogen charging followed by mechanical tests like Charpy resilience test, J integral and fatigue test were carried out [8, 9].

2 Electrochemical charging of hydrogen

Concerning electrochemical charging, a bibliographic review, summarized in Tables 1 and 2 [8–38] showed that some practical procedures were already available for hydrogen charging on steels used for pipeline or pressure vessels although they did not seem applicable to specimens with dimensions required for mechanical standards and testing, in fact, only three of them [29, 30, 32] used specimens 10 mm thick or more.

Solutions used were mostly acidic although also synthetic sea water and even NaOH solution were used. Among available hydrogen entry promoters (recombination poisoners) at different concentration, arsenic compounds were preferred due to their chemical and physical stability in these solutions. Electrochemical methods generally employ current densities in between 0.02 and 1000 $mA\ cm^{-2}$. The measured hydrogen content was rather scattered from 0.1 to almost 20 ppm. The wide measurement scattering of more than 2 orders of magnitude is in part attributable to some influencing parameters, such as applied current, time, sample thickness, pH and type of recombination poisoner used.

Newman and Shreir’s paper [17] is the most complete, accurate and reliable. These authors charged small steel cylinders of 2.54 mm in diameter using an electrochemical procedure in different solutions with pH ranging from 1.2 to 13. As, S, Se, Te, P were used as hydrogen entry promoters at different concentrations; S was the most effective in buffered acetic solution at pH about 4.6. pH resulted a very critical parameter in controlling the effectiveness of the promoter and even a small change showed a huge effect on the total absorbed hydrogen content. On the contrary, S^{2-} concentration (at least if higher than 60 ppm) did not result as a critical parameter. A complete removal of oxygen was obtained by fluxing solutions with high purity nitrogen and a current density optimized to 0.5 $mA\ cm^{-2}$. No information regarding the counter electrode material were reported.

The purpose of the present work is to set up an electrochemical method for hydrogen charging of thick steel specimens. The hydrogen charging can be divided into three steps:

1. Production of a large amount of atomic hydrogen on the material surface available for absorption and diffusion into steel;
2. Diffusion of the atomic hydrogen into steel through the full thickness;
3. Hydrogen containment in the steel.

The *first step* is the electrochemical one and is controlled by the electrochemical parameters, i.e. current density and potential of steel, and by the use of a poisoner for inhibiting the hydrogen recombination reaction ($2\ H \rightarrow H_2$).

The *second step*, which is a physical one, is governed by the Fick’s laws so that it depends on the diffusion coefficient of hydrogen, the fugacity of hydrogen on the steel surface and time. Temperature affects the diffusion coefficient.

The *third step* is needed because in ferritic steels at room temperature, hydrogen not bonded to high energy traps, diffuses fast enough to have an almost complete degassing of a specimen 1–2 cm thick in one day, a containment of hydrogen is necessary. This can be done according to a deep cooling of the sample by immersion in liquid nitrogen (thus reducing the diffusion coefficient).

Table 1 Maximum dimension, material and solution used for electrochemical H charging [10–46]

Ref	Maximum dimension (mm)	Steel	Solution
[8]	ND	API 5 L X70	0.5 M H ₂ SO ₄ + 250 mg/l NaAsO ₂
[9]	ND	API 5 L X70 different heat treatment conditions	0.5 M H ₂ SO ₄ + 100 ppm As ₂ O ₃
[20]	ND	carbon steel	2.5 mg/l H ₂ SeO ₃ + 0.1 N H ₂ SO ₄
[31]	Thickness = 0.05	Pure iron and HT-80 steel	0.5 M H ₂ SO ₄ + 5 mg/l As ₂ O ₃
[33]	Thickness = 0.25	AISI 1045 steel	1 N H ₂ SO ₄ + 5 mg/L As ₂ O ₃
[34]	Thickness = 0.5	API 5 L X100	0.05 M H ₂ SO ₄ + 250 mg/l As ₂ O ₃
[35]	Thickness = 1	API C90	0.5 M H ₂ SO ₄ + 250 mg/l As ₂ O ₃
[39]	Thickness = 1	ARMCO	NACE = 5% NaCl + 0.5% CH ₃ COOH + H ₂ S
[36]	Thickness = 1.1	Dual-phase steel	0.5 M H ₂ SO ₄ + 1 g/l thiourea
[37]	Thickness = 1.2	API 5 L X70 steel	0.5 M H ₂ SO ₄
[38]	Thickness = 1.3	API 5 L X70	NACE A = 5% NaCl + 0.5% CH ₃ COOH + H ₂ S different press. (pH = 2.5–6.0)
[40]	Thickness = 1.3	API 5 L X70	NACE A = 5% NaCl + 0.5% CH ₃ COOH + H ₂ S 1 atm (pH = 2.5–6.0)
[10]	Thickness = 1.5	Low C steel	Various pH + 10–3/10–1 mol/L Na ₂ S
[41]	Thickness = 1.5	API 5 L X80	0.5 M H ₂ SO ₄ + 0.25 g/L As ₂ O ₃
[39]	Thickness = 0.18–1.65	Fe ARMCO	0.5 M H ₂ SO ₄
[12]	Thickness = 2	API 5 L X100	0.1 M + H ₂ S gas saturated
[13]	Thickness = 2	Low carbon ferritic steel	3% NaCl + 3 g/l NH ₄ SCN
[14]	Thickness = 2	C-Mn steel	1 N H ₂ SO ₄ + 250 mg/l As ₂ O ₃
[15]	Thickness = 2	HSLA-80 and HSLA-100	Synthetic sea Water
[16]	Thickness = 2.5	3.5NiCrMoV steel	0.1 M NaOH
[16]	Thickness = 2.5	3.5NiCrMoV steel	0.1 M Na ₂ SO ₄
[17]	Φ = 2.54	Normalized HS steel	Various pH and promoters
[46]	Φ = 3.21	API 5 L X70	0.5 M H ₂ SO ₄ + 5 g/l KH ₂ AsO ₄
[46]	Φ = 3.21	API 5 L X70	0.5 M H ₂ SO ₄ + 5 g/l KH ₂ AsO ₄
[18]	Φ = 3.8	N80 steel	0.5 M CH ₃ COOH + 0.01 M Na ₂ S
[19]	Φ = 4	Pressure vessel C-steel	HCl solution
[21]	Φ = 4	AISI 420 steel	0.1 M H ₂ SO ₄
[42]	Φ = 4	Pressure vessel C-steel	1 N H ₂ SO ₄ + 0.25 g/L As ₂ O ₃
[23]	Thickness = 4	API 5 L X70	0.5 M H ₂ SO ₄
[24]	Φ = 5	0.05 C–0.20 + various alloys	3% NaCl
[25]	Φ = 5	C-Mn steel	3% NaCl + 3 g/l NH ₄ NCS
[43]	Thickness = 5	API 5 L X65	Sol ₁ = 1 N H ₂ SO ₄ + SeO ₂ , Sol ₂ = NACE + 1 bar H ₂ S, Sol ₃ = NACE + H ₂ S various pressures
[26]	Thickness = 5	C-Mn steel	NACE = 5% NaCl + 0.5% CH ₃ COOH + H ₂ S
[26]	Φ = 6	/	0.5 M H ₂ SO ₄ + 200 mg/l As ₂ O ₃
[27]	Φ = 6	Mild steel, Maraging steel grade 350	1% NaOH + 1 g/l As ₂ O ₃
[28]	Φ = 6	AISI 4135	3% NaCl + 0.3% NH ₄ SCN
[28]	Φ = 6	AISI 4135	0.1 N NaOH
[38]	Φ = 6	API 5 L X70	0.5 M H ₂ SO ₄ + 200 mg/L As ₂ O ₃
[29]	Φ = 10	AISI 4135	0.1 N NaOH
[30]	Φ = 12.7	High strength alloyed steels	1 M CH ₃ COOH + 1 M NaHCO ₃ + 15 ppm As ₂ O ₃ (pH 4.8)
[32]	Thickness = 16	C-steel with Ti	1 N H ₂ SO ₄ + 10 g/L As ₂ O ₃

Table 2 Experimental parameters and hydrogen content in literature experiments [10–46]

Ref	Current density (mA cm ⁻²)	Time (h)	H content (ppm)
[8]	$i = 50$	3	ND
[9]	$i = 0.1$	1	ND
[20]	$i = 10$	1 to 8	ND
[31]	$i = 50$	0.5	29.5
[33]	$i = 4.5$	ND	ND
[34]	$i = 50$	1, 3, 5	9, 10, 13
[35]	$i = 1-80$	24	up to 15.8
[39]	$i = 0.5-2$	ND	Permeation curves
[36]	$i = 0.8$	0.5 to 3	6.3 max (2.3 diffusible)
[37]	$i = 0-70$	2	0.9 to 11.5
[38]	$i = 1-2$	24 to 48	0 to 2.8
[40]	$i_1 = 1$ $i_1 = 1.5$ $i_3 = 2$	48	$Test_1 = 1.6$ $Test_2 = 3$ $Test_3 = 4.5$
[10]	ND	ND	ND
[41]	$i_1 = 2$ $i_2 = 4$ $i_3 = 6$ $i_4 = 10$ $i_5 = 15$ $i_6 = 20$	48	$Test_1 = 2.52$ $Test_2 = 4.15$ $Test_3 = 5.75$ $Test_4 = 10.1$ $Test_5 = 11.88$ $Test_6 = 14.81$
[39]	$i = 1-10$	3	ND
[12]	$i = 10-100$	20	2 to 18
[13]	$i = 1$	12	ND
[14]	$i = 10$	3	3.94
[15]	Cathodic potential	2	1 to 2.2
[16]	Various potentials	24	0,704 to 1.038
[16]	Various potentials	24	0.987 to 1.682
[17]	$i = 0.5$	24	Depends on pH and promoter
[46]	$i = 70$	0.25	ND
[40]	$i = 10-66$	0.25	ND
[18]	$i = 0.3$	50	1
[19]	$i = 5$	24	ND
[21]	$i = 8$	1–125	ND
[42]	$I_1 = 10$ $i_2 = 1$	0.5	$Test_1 = 2.4$ $Test_2 = 1.1$
[23]	$i = 10-1000$	48	0.3 to 8
[24]	$i = 0.3$	1	ND
[25]	$i = 0.02-1.0$	variable	max 1.6 ppm with TDS, at time 0s 1 ppm
[43]	Variable	variable	0.91 to 2.93
[26]	NACE test	96	$Test_1 = 1.9$ $Test_2 = 1.6$ $Test_3 = 0.8$ $Test_4 = 0.8$
[27]	$i = 4$	5 and 30	4.5
[27]	$i = 15$	24	ND
[28]	$i = 0.3-30$	1 to 72	up to 1.3
[28]	$i = 0.3$	1 to 72	up to 0.13
[38]	$i = 0.4$	0.1 to 0.5	4.5
[29]	$i = 0.03-1$	48	0.1 to 0.4
[30]	ND	ND	ND
[32]	$i = 0.02$	24	ND

3 Experimental setup

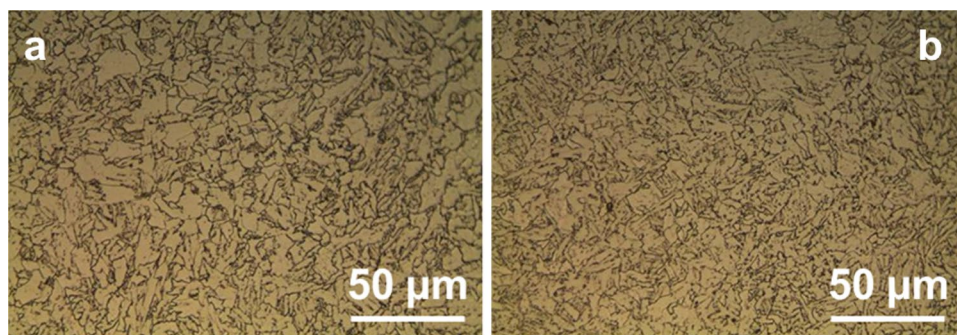
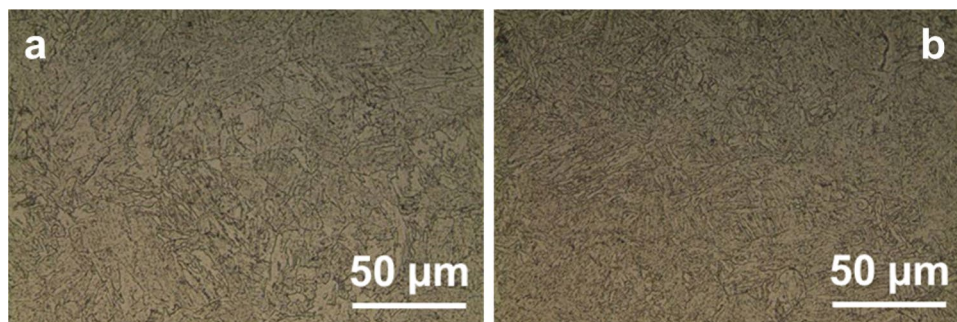
3.1 Materials

Steels tested were:

- Micro-alloyed C-Mn steel, X65 grade (323 mm OD × 46 mm WT);

- 2.5 Cr 1 Mo steel, namely F22 (230 mm OD × 65 mm WT).

Taken from seamless pipes in quenched and tempered conditions. X65 grade pipe was a pipe from conventional billet casting—piercing—hot rolling—quench and tempering operations. F22 pipe was a pipe from ingot casting—forging—piercing—hot rolling—quench and tempering

Fig. 1 Microstructure of X65 steel: centre (a) internal (b)**Fig. 2** Microstructure of F22 steel: centre (a) internal (b)**Table 3** Chemical composition (weight%)

Steel	Element							
	C	Mn	Cr	Mo	Ni	Nb	V	Ti
X65	0.11	1.18	0.17	0.15	0.42	0.023	0.06	<0.01
F22	0.14	0.43	2.25	1.04	0.08	0.023	<0.01	<0.01

production route. Both materials are for sour service use, so that they underwent through all the required qualifications. Table 3 reports the chemical compositions of the steels tested.

X65 steel microstructure is equiaxed and acicular ferrite with finely dispersed carbides, as shown in Fig. 1. The microstructure is rather homogeneous, no differences are visible among different alignments (internal, centre, external) or different orientations (longitudinal, transversal). Inclusion shape is round as it is expected for a “sour gas” material treated with calcium in order to have only spheroidized inclusions (type D globular inclusions) and no elongated inclusions are present. Longitudinal and transverse orientation don’t show any difference neither as density nor as mean diameter (1.5 μm long. surface, 1.4 μm transv. surface); no central segregation is present.

F22 steel microstructure is typical of tempered lath martensite, i.e. elongated ferrite grains with finely dispersed carbides (Fig. 2). Metallographic attacks also show prior-austenitic grains; the microstructure is rather homogeneous, no differences are visible among different alignments or different orientations (longitudinal, transversal).

Inclusion density is very low; material has been treated with calcium and inclusion shape is round (type D globular inclusions) and no elongated inclusions are present; longitudinal and transverse orientation don’t show any difference neither as density nor as mean diameter (1.2 μm long. surface, 1.3 μm transversal surface); no central segregation is present.

Microhardness was measured. For X65, mean value of 209.5 ± 12.1 HV and Yield Strength 511 MPa Ultimate Tensile Strength 609 MPa [7]) in the expected range for an X65 steel (531–758 MPa), hardness is rather homogeneous on both internal and external surfaces while it is lower on the centreline. For F22 steel, mean value of 210.3 ± 11.7 HV and Yield Strength 468 MPa (Ultimate Tensile Strength 592 MPa [7]), hardness is rather homogeneous through the thickness.

3.2 Specimens

- To facilitate the measurement of absorbed hydrogen, two kinds of specimens were used: prismatic specimens having

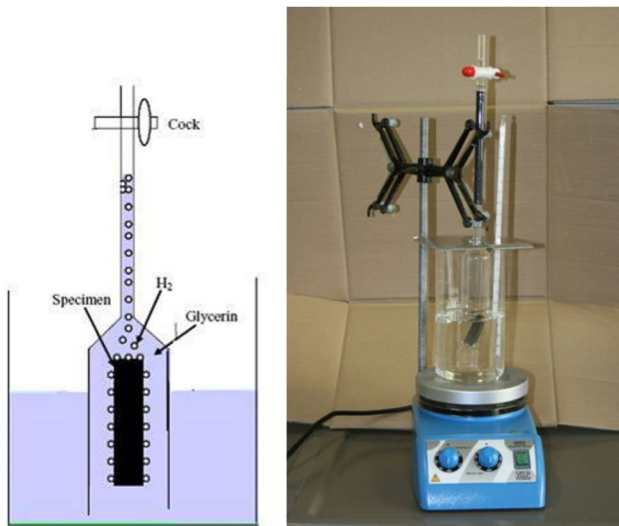


Fig. 3 Measurement of hydrogen content by hot glycerol bath

a cross section of $10 \times 10 \text{ mm}^2$ equal to Charpy specimens and length 40 mm.

- Cylindrical specimens having a much smaller cross section (height 9 mm, diameter 5 mm).

The prismatic specimen could contain up to some cm^3 of hydrogen that can be measured by using the hot glycerol bath (described in Sect. 3.4), while hydrogen in small cylindrical specimens were measured by two external laboratories by means of IGF Inert gas fusion [44] using a commercial hydrogen analyser LECO [45].

After the adjustment of the hydrogen charging method, different type of specimens were charged: Charpy CV, J integral or fatigue crack propagation Compact Tension (CT) specimens [6, 7]. The net thickness of the CT specimen, considering the reduction in thickness according to the presence of side grooves obtained by electro erosion, is $16 \text{ mm} \pm 0.05 \text{ mm}$.

3.3 Hydrogen charging

Preliminary tests on hydrogen charging were carried out in a cell with volume of 1 L and the counter electrode is made by an activated titanium net.

The solution adopted is:

- 0.2 mol L^{-1} of CH_3COOH ($12.0 \text{ g/L} = 11.6 \text{ mL/L}$).
- 0.2 mol L^{-1} of CH_3COONa (16.4 g/L).
- The solution is buffered at pH 4.8.
- 1.5 g/L of $\text{Na}_2\text{S} \cdot 9\text{H}_2\text{O}$ equivalent to 200 ppm of sulphide as S^{2-} .

Hydrogen charging was carried out at room temperature, at a current density of 0.6 mA cm^{-2} , for 20 h. The solution contained atmospheric oxygen.

Before hydrogen charging the specimens were treated as following:

- Mechanical polishing with emery paper (up to 600 mesh).
- Degreasing in trichloroethylene for 5' with ultrasounds,
- Pickling in concentrated HCl solution (37%) for 5' with ultrasounds,
- Rinsing in distilled water,
- Final rinsing in ethylic alcohol.

The most critical factors influencing hydrogen charging procedure resulted the following: current density, presence of oxygen, solution composition and its modification during the tests, type of counter electrode and charging time.

Current density was fixed at a low value, as in [17, 46], in order to have a good level of produced hydrogen, avoiding hydrogen bubble turbulence. In fact, the higher the current density, the lower will be the absorbed hydrogen in proportion to the total charge measured during the whole charging process. This could be a consequence of the increasing hydrogen evolution on steel surface, which creates turbulence and large gas bubbles on the surface partially shielding

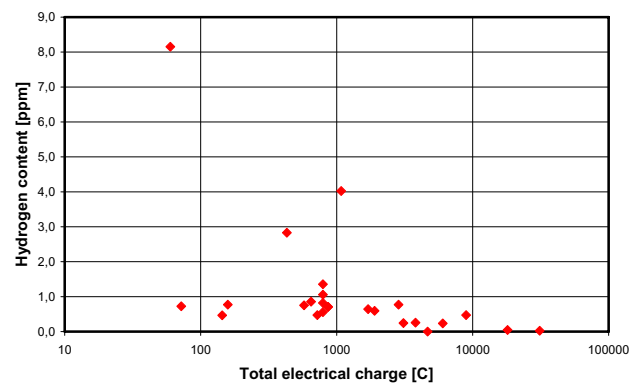


Fig. 4 Hydrogen released from specimen in glycerol bath Vs. total electrical charge

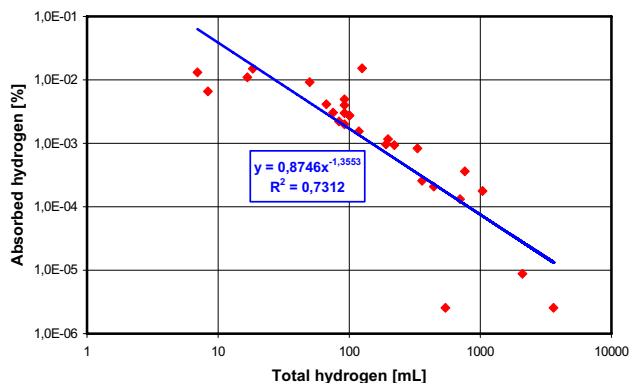


Fig. 5 Charging “efficiency” Vs. total produced hydrogen (Log-Log diagram)

it, leading to an inhomogeneous current distribution thus reducing the overall hydrogen penetration. Furthermore H_2S (stable at low pH) can move to cathodic surface only by diffusion and can be easily stripped by a gas flow (nitrogen, hydrogen).

The presence of oxygen as cathodic reaction is negligible (oxygen limiting current density much lower than current density applied); however, oxygen oxidizes sulphides to sulphur or to other oxidized species, as it is clearly demonstrated by the changing of the solution appearance, which became milky as sulphides are added to the solution. A long degassing procedure with flux of 99.99% purity nitrogen, according to [8] was used.

The composition of the solution was modified during the research: sulphide content was increased to 600 ppm in order to guarantee a residual presence of sulphides high enough to have the expected effect on the inhibition of hydrogen recombination during charging. Moreover, the pH of the solution was decreased to 4.3 to increase the stability of H_2S in solution [17].

In order to reduce any possible effects of solution modification during hydrogen charging two actions were adopted: increasing the ratio of the solution volume to specimen surface and increasing the anode surface. The solution modification depends on the total circulated charge during one charging operation, being current and charging time equal their faradic effects on the solution will be diluted the larger is the solution volume. Moreover, increasing the anode surface the anodic overvoltage will decrease and spurious uncontrolled reactions will be less probable.

The anode material is also important, because the anodic potential can influence oxidation of other species in solution.

The charging conditions adopted at the end of the experiments are the following:

- 0.4 mol/L CH_3COOH (24.0 g/L = 23.2 mL/L).
- 0.2 mol/L CH_3COONa (16.4 g/L).
- The solution is buffered at pH 4.3.
- 4.5 g/L of $Na_2S \cdot 9H_2O$ equivalent to 600 ppm of sulphide as S^{2-} .
- De-aerated solution.
- Room temperature.

The current density is 0.6 mA cm^{-2} , for 20 h.

The volume of the test cell has been increased to 5 L (CV specimens) or 10 L (CT specimens). Also the anode material was changed. Initially, zinc and aluminium were tried as possible candidates; however, the final choice fell over magnesium because its anodic potential under current is lower and oxidation of other species in solution is less probable.

The same method was found to be effective for electrochemical H charging of low-alloy Cr-Mo steel for pressure vessel [47].

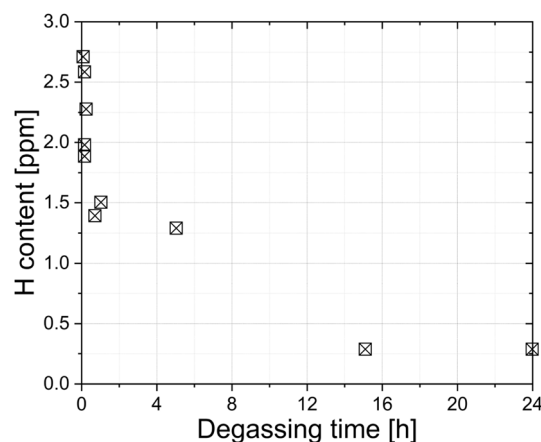


Fig. 6 Evolution of the absorbed H as a function of the degassing time for AISI 4130 [48]

3.3.1 Treatment after hydrogen charging

After hydrogen charging, in order to prevent hydrogen, escape the specimens were inserted into liquid nitrogen in order to drop the hydrogen diffusion coefficient. Following this idea, the specimens were immersed after 30''–45'' after the hydrogen charging, and the maximum conditioning time to reach the temperature was 3 min for CT specimens. By using this approach, it was possible to reduce the time needed for the hydrogen charging and to increase the number of specimens charged (until 12 CV or 4 CT specimens in 24 h). Preliminary tests were also carried out plating the specimens with a layer of FCC material (Cu and Ni) which has a hydrogen diffusion coefficient at least two orders of magnitude lower than ferritic steel. Finally, the immersion in liquid nitrogen was selected.

3.4 Hydrogen measurement

Measurement of hydrogen in steel is rather complex, normally the specimen must be heated at a temperature high enough to release hydrogen that can be measured in different ways. Since hydrogen is trapped into steel in various sites at progressively increasing energy levels, this means that the higher the trapping energy the higher the temperature needed to release hydrogen from the steel specimen.

In case of sour grade steel having a very low inclusion level, as the material under study, it is expected that most of absorbed hydrogen is present in reversible traps (grain boundaries, dislocations, etc.), therefore in order to have a quick and simple evaluation of the hydrogen content the method of hot glycerol bath was adopted (Fig. 3) although this method underestimates the hydrogen content for two reasons: it measures only hydrogen which is released at a temperature below $200 \text{ }^\circ\text{C}$ and part of this hydrogen can

Table 4 Experimental parameters of hydrogen charging of three different test sets of specimens subjected to the measurement of hydrogen content

	I [A]	Time [h]	Volume (L)	Anode area [cm ²]	Charge [C]	C/V [C/l]	i_a [mA cm ⁻²]
Laboratory 1 –series 1	0.003	20	0.9	40	216	240	0.0750
Laboratory 1 –series 2	0.007	20	5.0	1800	504	100.8	0.0039
Laboratory 2 –series 3	0.044	20	5.0	1800	3168	633.6	0.0244

Table 5 Mean hydrogen content (LECO, external laboratory 1) of specimens with different charging time (series 1, two specimens for each condition)

Specimen set	Charging time [h]	Hydrogen content [ppm]
0	0 (As received)	0.2
1	168	1.9
2	20	2.5
3	4	2.0

Table 6 Hydrogen content (LECO, external laboratory 1) of specimens charged (series 2)

Specimen	Hydrogen content [ppm]
01	14.1
02	15.6
04	11.9
05	22.7
06	7.6
07	24.7

Table 7 Hydrogen content of specimens (series 3)

Set	Specimen	Hydrogen content [ppm]	
		LECO*	Glycerol bath
1	9		1.1
1	2	2.2	
1	4	0.54	
1	13	0.7	
2	1		0.6
2	11	<0.1	
2	12	0.53	
2	8	<0.1	

* external laboratory 2 (Centro Sviluppo Materiali S.p.A., ROMA, Italy)

dissolve into glycerol, then for low hydrogen content the error can be rather high.

According to [31] glycerol bath method can underestimate the real amount of diffused hydrogen of 30–60%, with

greater error for low hydrogen volumes adsorbed. In spite of this, this method is still widely used, and was adopted because it allows a very easy preliminary evaluation of hydrogen content and, due to the very low inclusion content of the studied steels, it is expected that most of the hydrogen is easily diffusible, and it is reasonable to expect that it is released below 200 °C.

As already introduced control measurement was performed in external laboratories, using a commercial IGF instrument (LECO), on two types of specimens, small cylindrical and prismatic.

3.5 Mechanical tests

Fracture mechanics tests were carried out on standard CT specimens, according to ASTM 1820 [48]. An optimized thickness of 20 mm was selected in order to guarantee plane strain condition, during the mechanical test, and an agile hydrogen charging (being the latter process much easier in thin samples). Side grooves were machined on the specimens, along the crack propagation direction, in order to reduce the plane stress condition [6, 49]. During the J-integral tests J_Q values were evaluated considering the 0.2 mm offset line criterion. The test was performed at different temperatures by feeding a blend of liquid nitrogen and alcohol. To check the specimen temperature in the bulk, before and during tests, a small hole was machined in the specimens and a T-type thermocouple was welded in, without interfering with the test.

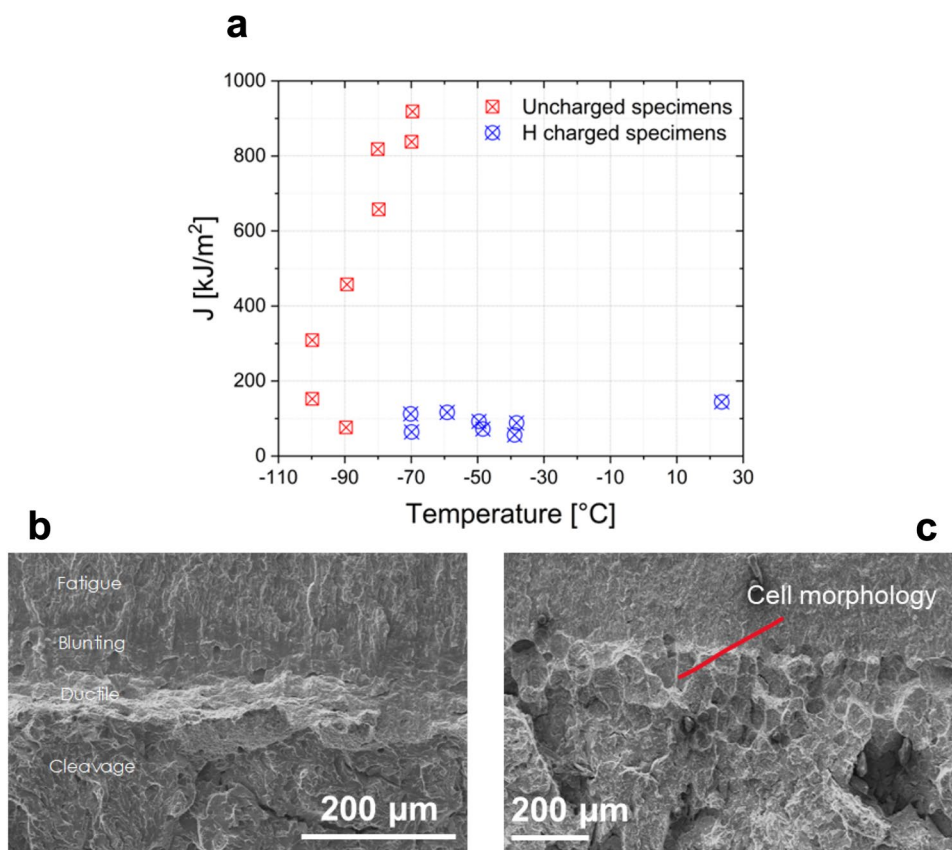
4 Results and discussion

4.1 Hydrogen charging

The charging conditions of the specimens subjected to the measurement of the hydrogen content are reported in Table 4 and the results of the hydrogen measurements are reported in Tables 5, 6 and 7 and in Figs. 4 and 5.

Charging time determines the total amount of produced hydrogen at a given current intensity (Faraday's law) and the amount of atomic hydrogen penetrated into the steel specimens (2nd Fick's law), then increasing charging time one should expect an increasing of the dissolved hydrogen.

Fig. 7 Fractographic analysis of X65 specimen after J integral test **a** without hydrogen **b** and H charged **c**



If we consider all the results obtained in very different charging conditions, as reported in Fig. 4, it is possible to observe that when the total charge increases (longer times or higher current densities), the portion of hydrogen dissolved in the steel sample (measured by hot glycerol bath) with respect to the total amount evolved decreases. The ratio of the absorbed hydrogen vs. the total produced hydrogen during charging, calculated from the total electric charge with the Faraday's law, decreased roughly with a hyperbolic law (Fig. 5). This ratio could be defined as the “charging efficiency” of the process. A possible reason of this behaviour is that the circulation of electric current and in particular anodic reactions have an effect in progressively reducing the sulphide content in the solution then if from one side longer charging time increase hydrogen production on the other increase sulphide consumption increase and the effect of promoter fall to zero. The results shown in Figs. 4 and 5 were confirmed by the first set of hydrogen measurement on small cylindrical specimens ($\Phi = 5$ mm) made by an external laboratory (OMECO S.r.l, Monza, Italy) using commercial IGF “LECO” hydrogen analyser (Table 5).

The effect of the size of the specimen is very important because small specimens, used in most of the published research, need a very small amount of hydrogen to reach the equilibrium condition for the specific chemical-physical

parameters adopted, moreover hydrogen diffusion in thin specimens is very fast and a short time is needed to saturate the whole thickness. Therefore saturation of small specimens with hydrogen can be reached in short time, the electrical charge is low, it is easy to obtain a high ratio of the volume of the charging solution to the specimen surface and then the solution modification during charging is negligible.

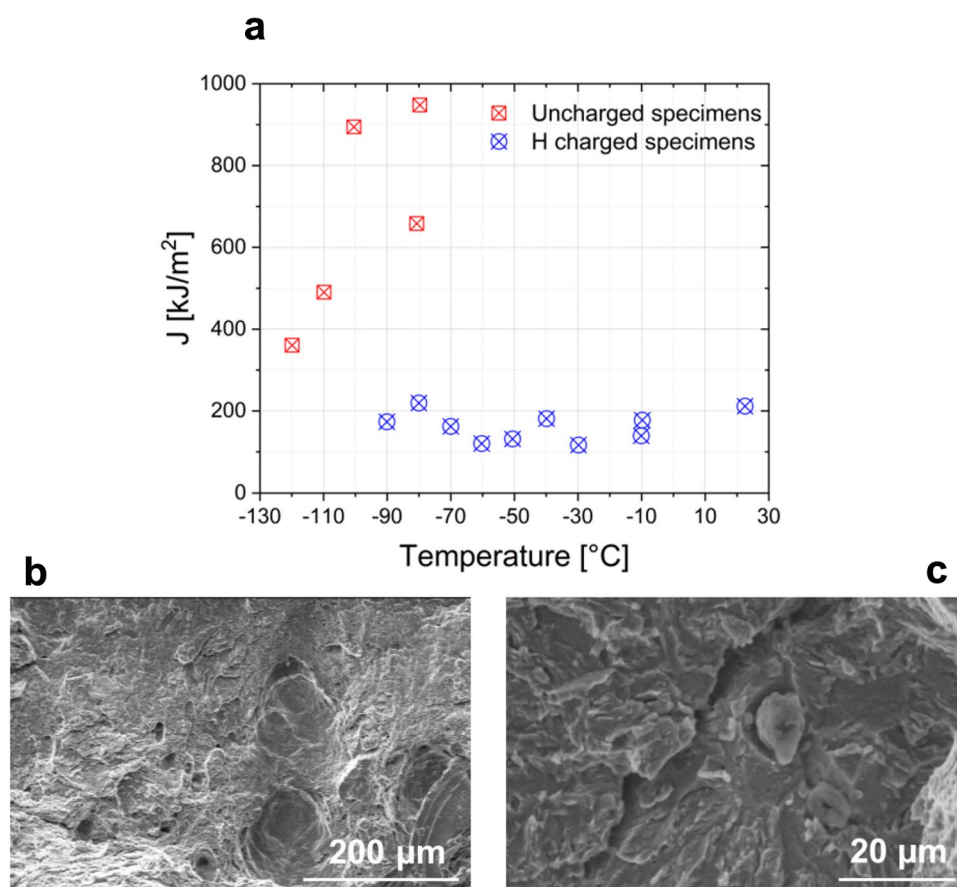
The results obtained in our experimental work (Tables 5, 6 and 7), by taking into account the different charging conditions in Table 4, allows to state that the lower the C/V ratios (charge to solution volume) and i_a (anodic current density) the higher the hydrogen content.

Finally, Table 7 refers to two sets of 4 specimens each, from each set one specimen was evaluated for hydrogen content in our laboratories with the glycerol bath method and the other three have been sent to an external laboratory (Centro Sviluppo Materiali S.p.A., Roma, Italy). The two methodologies are in general agreement although the scattering of the results.

It is possible to state that hydrogen content of the charged specimens is in the range $0.6 \div 2$ ppm. The present method was found to be effective also in case of H charging of low alloy Cr-Mo steel (AISI 4130), offering an H concentration always in between 2 and 3 wt.ppm [47].

It is also reported (see Fig. 6) the effect of degassing time (h) required to desorb H from charged samples of AISI 4130.

Fig. 8 Fractographic analysis of F22 specimen after J integral test **a** without hydrogen **b** and H charged **c**



It is possible to see how after 5 h of degassing, a considerable amount (~ 1.3 ppm) of atomic H was still retained inside the metal, while after 24 h from the charging procedure permit to obtain low values ~ 0.3 ppm.

4.2 Mechanical tests and fracture surface examination

The specimens charged with hydrogen with the electrochemical methods (hydrogen content in the range 0.6–2 ppm) have been subjected to mechanical testing. Hydrogen induced mechanical properties variation of the material are more evident if the fracture toughness J–R curves are considered, while for impact test the results were not significantly affected by the presence of hydrogen [8]. When the material is charged with hydrogen, in fact, J_Q (material fracture toughness) values decreased significantly with respect to the values obtained in the uncharged conditions. Figure 7a shows the measured values of J_Q vs. T for X65 steel with and without H. J_Q values of uncharged X65 specimens are larger than 900 kJ/m^2 to a temperature of $T = -70 \text{ }^\circ\text{C}$ then they start to decrease. During the tests the cracks never propagate in an unstable way and also the stable crack propagation is very small. The plastic zone at the crack tip is very extended

and the crack tip blunts without propagation. The J_Q values of hydrogen charged specimens are significantly lower, reaching a plateau around 150 kJ/m^2 in all the experimented temperature range to the room temperature. Similar considerations can be added in case of F22 steel: Fig. 8a shows that the J_Q values of the hydrogen charged specimens are significantly lower with respect to the uncharged ones. It is possible to notice how J_Q values of the uncharged sample are temperature dependent and subjected to a decrease for T lower than $-80 \text{ }^\circ\text{C}$. On the other hand, the H charged samples present almost constant J_Q values ($J_Q \sim 90 \text{ kJ/m}^2$) with the temperature in the range -80 to $25 \text{ }^\circ\text{C}$. Here some fractographic analysis of the specimens after J integral tests are presented with the aim to underline the different behaviour of hydrogen free and hydrogen charged specimens. In Fig. 7b the behaviour of steel X65 without hydrogen is shown: fracture surface shows fatigue morphology, blunting, ductile propagation and cleavage (final breaking of the specimens in liquid nitrogen). In the specimen charged with hydrogen the fracture surface is quite different: the blunting zone is less evident, and the stable propagation zone shows a “cell” morphology (Fig. 7c): inside the cell the fracture surface is brittle, and, in the borders, ductile morphology

is evident. In most cases inclusion is noticed at the centre of the “cell”.

In Fig. 8 fractographic analysis of F22 specimens is shown. In the specimen without hydrogen (Fig. 8b) ductile fracture surface is observed, while in the hydrogen charged (Fig. 8c) scenario it is possible to observe the stable propagation zone (“cell” morphology), displaying a length of several mm [6].

In this paper only a brief outline of the results of the mechanical tests was presented. For more details about the experiments concerning J integral and fatigue crack propagation rate it is possible to refer to [7, 47].

5 Conclusion

An electrochemical method to obtain hydrogen charging on large steel specimens was set up after investigating the main influencing factors: test solution (composition and pH), current density, charging time and solution volume to cathodic and anodic area ratio.

Hydrogen charging was carried out in acetic acid and sodium acetate solution with 200 to 600 ppm S^{2-} added, at room temperature, in de-aerated solution; applied cathodic current density was 6 A m^{-2} for 20 h. Escaping of hydrogen by diffusion was prevented by immersion in liquid nitrogen in order to guarantee that the hydrogen penetrated into the specimen should remain confined in the material for a time long enough to carry out mechanical tests.

Hydrogen content in the range from 0.6 to 2 ppm was measured by two different methods: hot glycerol bath and IGF-Inert gas fusion. Although the scattering of the results, the results of the two methods are in good agreement.

The specimens charged with hydrogen show a decrease of fracture toughness vs. specimens not charged, for both tested materials and all testing temperatures.

Fracture surface after mechanical testing (J integral) show significant differences between the specimens charged with hydrogen and those without hydrogen demonstrating this test to be particularly sensitive to H effect on metals.

Acknowledgements This work was supported by ENI-Exploration and Production Division. The authors would like to thank Giorgio Re, Gabriele Fumagalli, Luciano Lazzari and Patrizia Fassina for their scientific contribution.

Author contributions LC Conceptualization, experimental design, data collection, editing, writing. LP Experimental design, data collection, experimental design. FB Editing, writing, experimental design. MO Editing, writing, experimental design.

Funding Open access funding provided by Politecnico di Milano within the CRUI-CARE Agreement.

Declarations

Competing interests The authors declare that they have no known competing financial interests or personal relationships that could have appeared to influence the work reported in this paper.

Open Access This article is licensed under a Creative Commons Attribution 4.0 International License, which permits use, sharing, adaptation, distribution and reproduction in any medium or format, as long as you give appropriate credit to the original author(s) and the source, provide a link to the Creative Commons licence, and indicate if changes were made. The images or other third party material in this article are included in the article's Creative Commons licence, unless indicated otherwise in a credit line to the material. If material is not included in the article's Creative Commons licence and your intended use is not permitted by statutory regulation or exceeds the permitted use, you will need to obtain permission directly from the copyright holder. To view a copy of this licence, visit <http://creativecommons.org/licenses/by/4.0/>.

References

- San Marchi C, Somerday BP, Robinson SL (2007) Permeability, solubility and diffusivity of hydrogen isotopes in stainless steels at high gas pressures. *Int J Hydrogen Energy* 32:100–116. <https://doi.org/10.1016/j.ijhydene.2006.05.008>
- Pedferri P (2018) Corrosion science and engineering. Springer, New York
- Oriani RA, Hirth JP, Smialowski M (1986) Hydrogen degradation of ferrous alloys. *Corrosion* 43(7):390–397
- Moss W (2009) Guidelines on materials requirements for carbon and low alloy steels for H_2 -containing environments in oil and gas production, 3rd edn. Routledge, London
- Gangloff RP, Somerday BP (2012) Gaseous hydrogen embrittlement of materials in energy technologies: the problem its characterisation and effects on particular alloy classes. Elsevier, Amsterdam
- Fassina P, Brunella MF, Lazzari L, Re G, Vergani L, Sciuccati A (2013) Effect of hydrogen and low temperature on fatigue crack growth of pipeline steels. *Eng Fract Mech* 103:10–25. <https://doi.org/10.1016/j.engfracmech.2012.09.023>
- Fassina P, Bolzoni F, Fumagalli G, Lazzari L, Vergani L, Sciuccati A (2012) Influence of hydrogen and low temperature on mechanical behaviour of two pipeline steels. *Eng Fract Mech* 81:43–55. <https://doi.org/10.1016/j.engfracmech.2011.09.016>
- Saleh AA, Hejazi D, Gazder AA, Dunne DP, Pereloma EV (2016) Investigation of the effect of electrolytic hydrogen charging of X70 steel: II. Microstructural and crystallographic analyses of the formation of hydrogen induced cracks and blisters. *Int J Hydrogen Energy*. <https://doi.org/10.1016/j.ijhydene.2016.05.235>
- Torres-Islas A, Salinas-Bravo VM, Albarran JL, Gonzalez-Rodriguez JG (2005) Effect of hydrogen on the mechanical properties of X-70 pipeline steel in diluted $NaHCO_3$ solutions at different heat treatments. *Int J Hydrogen Energy* 30:1317–1322. <https://doi.org/10.1016/j.ijhydene.2005.04.007>
- Kawashima A, Hashimoto K, Shimodaira S (1976) Hydrogen electrode reaction and H embrittlement of mild steel in hydrogen sulfide solutions. *Corrosion*. <https://doi.org/10.5006/0010-9312-32.8.321>
- Zhang T, Chu WY, Gao KW, Qiao LJ (2003) Study of correlation between hydrogen-induced stress and hydrogen embrittlement. *Mater Sci Eng A*. [https://doi.org/10.1016/S0921-5093\(02\)00600-7](https://doi.org/10.1016/S0921-5093(02)00600-7)

12. Jin TY, Liu ZY, Cheng YF (2010) Effect of non-metallic inclusions on hydrogen-induced cracking of API5L X100 steel. *Int J Hydrogen Energy*. <https://doi.org/10.1016/j.ijhydene.2010.05.089>
13. Nagumo M, Ishikawa T, Endoh T, Inoue Y (2003) Amorphization associated with crack propagation in hydrogen-charged steel. *Scr Mater*. [https://doi.org/10.1016/S1359-6462\(03\)00469-X](https://doi.org/10.1016/S1359-6462(03)00469-X)
14. Zhao Y, Seok MY, Choi IC, Lee YH, Park SJ, Ramamurty U, Suh JY, Jang J (2015) II the role of hydrogen in hardening/softening steel: influence of the charging process. *Scr Mater*. <https://doi.org/10.1016/j.scriptamat.2015.05.017>
15. Banerjee K, Chatterjee UK (2001) Hydrogen permeation and hydrogen content under cathodic charging in HSLA 80 and HSLA 100 steels. *Scr Mater*. [https://doi.org/10.1016/S1359-6462\(00\)00594-7](https://doi.org/10.1016/S1359-6462(00)00594-7)
16. Venezuela J, Tapia-Bastidas C, Zhou Q, Depover T, Verbeken K, Gray E, Liu Q, Liu Q, Zhang M, Atrens A (2018) Determination of the equivalent hydrogen fugacity during electrochemical charging of 3.5NiCrMoV steel. *Corros Sci*. <https://doi.org/10.1016/j.corsci.2017.12.018>
17. Newman JF, Shreir LL (1969) Role of hydrides in hydrogen entry into steel from solutions containing promoters. *Corros Sci* 9:631–641. [https://doi.org/10.1016/S0010-938X\(69\)80117-4](https://doi.org/10.1016/S0010-938X(69)80117-4)
18. Giuliani L, Mirabile M, Sarracino M (1974) Embrittlement kinetics of N 80 steel in H₂S environment. *Met Trans* 5:2069–2073. <https://doi.org/10.1007/BF02644500>
19. Strnadel B (1998) Failure of steels caused by hydrogen induced microcracking. *Eng Fract Mech* 61:299–310. [https://doi.org/10.1016/S0013-7944\(98\)00073-3](https://doi.org/10.1016/S0013-7944(98)00073-3)
20. Beloglazov SM (2003) Peculiarity of hydrogen distribution in steel by cathodic charging. *J Alloys Compd* 356–357:240–243. [https://doi.org/10.1016/S0925-8388\(03\)00354-2](https://doi.org/10.1016/S0925-8388(03)00354-2)
21. Biggiero G, Borruto A, Gaudino F (1995) Embrittlement due to hydrogen in ferritic and martensitic structural steels. *Int J Hydrogen Energy*. [https://doi.org/10.1016/0360-3199\(94\)E](https://doi.org/10.1016/0360-3199(94)E)
22. Wu XQ, Kim IS (2003) Effects of strain rate and temperature on tensile behavior of hydrogen-charged SA508 Cl.3 pressure vessel steel. *Mater Sci Eng A*. [https://doi.org/10.1016/S0921-5093\(02\)00737-2](https://doi.org/10.1016/S0921-5093(02)00737-2)
23. Wang R (2009) Effects of hydrogen on the fracture toughness of a X70 pipeline steel. *Corros Sci*. <https://doi.org/10.1016/j.corsci.2009.07.013>
24. Wei FG, Hara T, Tsuzaki K (2009) Nano-precipitates design with hydrogen trapping character in high strength steels. In *Proceedings of the International Hydrogen Conference—Effects of Hydrogen on Materials*;
25. Asahi H, Hirakami D, Yamasaki S (2003) Hydrogen trapping behavior in vanadium-added steel. *ISIJ Int*. <https://doi.org/10.2355/isijinternational.43.527>
26. Chatteraj I, Tiwari SB, Ray AK, Mitra A, Das SK (1995) Investigation on the mechanical degradation of a steel line pipe due to hydrogen ingress during exposure to a simulated sour environment. *Corros Sci*. [https://doi.org/10.1016/0010-938X\(95\)00001-Z](https://doi.org/10.1016/0010-938X(95)00001-Z)
27. Tiwari GP, Bose A, Chakravartty JK, Wadekar SL, Totlani MK, Arya RN, Fotedar RK (2000) A study of internal hydrogen embrittlement of steels. *Mater Sci Eng A*. [https://doi.org/10.1016/S0921-5093\(00\)00793-0](https://doi.org/10.1016/S0921-5093(00)00793-0)
28. Wang M, Akiyama E, Tsuzaki K (2007) Effect of hydrogen on the fracture behavior of high strength steel during slow strain rate test. *Corros Sci*. <https://doi.org/10.1016/j.corsci.2007.03.038>
29. Wang M, Akiyama E, Tsuzaki K (2006) Determination of the critical hydrogen concentration for delayed fracture of high strength steel by constant load test and numerical calculation. *Corros Sci*. <https://doi.org/10.1016/j.corsci.2005.07.010>
30. Pound BG (1998) Hydrogen trapping in high-strength steels. *Acta Mater*. [https://doi.org/10.1016/S1359-6454\(98\)00247-X](https://doi.org/10.1016/S1359-6454(98)00247-X)
31. Ohtsubo T, Goto S, Amano M (1985) Development of apparatus for determination of diffusible hydrogen in steel. *Trans Iron Steel Inst Japan*. <https://doi.org/10.2355/isijinternational1966.25.21>
32. Stevens MF, Bernstein IM (1989) Microstructural trapping effects on hydrogen induced cracking of a microalloyed steel. *Metall Trans A*. <https://doi.org/10.1007/BF02651657>
33. Oriani RA, Josephic PH (1980) Effects of hydrogen on the plastic properties of medium-carbon steels. *Metall Trans A* 11:1809–1820. <https://doi.org/10.1007/BF02655096>
34. Dong CF, Liu ZY, Li XG, Cheng YF (2009) Effects of hydrogen-charging on the susceptibility of X100 pipeline steel to hydrogen-induced cracking. *Int J Hydrogen Energy*. <https://doi.org/10.1016/j.ijhydene.2009.09.090>
35. Yu GH, Jiang BL, Qiao LJ, Wang Y, Bin; Chu WY (1997) Threshold stress intensity for hydrogen—induced cracking of tubular steel. *Scr Mater*. [https://doi.org/10.1016/S1359-6462\(97\)00037-7](https://doi.org/10.1016/S1359-6462(97)00037-7)
36. Depover T, Wallaert E, Verbeken K (2016) Fractographic analysis of the role of hydrogen diffusion on the hydrogen embrittlement susceptibility of DP steel. *Mater Sci Eng A*. <https://doi.org/10.1016/j.msea.2015.09.124>
37. Yan M, Weng Y (2006) Study on hydrogen absorption of pipeline steel under cathodic charging. *Corros Sci*. <https://doi.org/10.1016/j.corsci.2005.01.011>
38. Kim WK, Koh SU, Yang BY, Kim KY (2008) Effect of environmental and metallurgical factors on hydrogen induced cracking of HSLA steels. *Corros Sci*. <https://doi.org/10.1016/j.corsci.2008.09.030>
39. Antano-Lopez R (2003) Hydrogen Permeation in Iron Membranes under Various Charging Conditions Including Wet H₂S. In *Proceedings of the EUROCORR*;
40. Kim VK, Koh SU, Kim KY (2007) The Effect of Metallurgical Factors on HIC of High Strength Linepipe Steels. In *Proceedings of the Corrosion*;
41. Zhang T (2003) Study on correlation between hydrogen-induced stress and hydrogen embrittlement. *Mater Sci Eng A* 347(1–2):291–299
42. Wu XQ, Kim IS (2003) Effects of strain rate and temperature on tensile behavior of hydrogen-charged SA508 Cl.3 pressure vessel steel. *Mater Sci Eng A* 348:309–318. [https://doi.org/10.1016/S0921-5093\(02\)00737-2](https://doi.org/10.1016/S0921-5093(02)00737-2)
43. Schmitt G, Buschmann R, Sadlowsky B (2004) Hydrogen Permeation under Tensile Stress—Unexpected Effect of Stress on Hydrogen Cracking of Steel under Subcritical Charging. In *Proceedings of the Corrosion*;
44. Weiss Z (2021) Analysis of hydrogen in Inorganic materials and coatings: a critical review. *Hydrogen* 2:225–245. <https://doi.org/10.3390/hydrogen2020012>
45. Lawrenz D, Hawkins J Simultaneous Oxygen, Nitrogen and Hydrogen Determination of Metals. 1–11
46. Bolzoni F, Fassina P, Fumagalli G, Lazzari L, Re G (2010) Hydrogen charging of carbon and low alloy steel by electrochemical methods. In *Proceedings of the Eurocorr ; Moscow, 2010*
47. Colombo C, Fumagalli G, Bolzoni F, Gobbi G, Vergani L (2015) Fatigue behavior of hydrogen pre-charged low alloy Cr-Mo steel. *Int J Fatigue* 83:2–9. <https://doi.org/10.1016/j.ijfatigue.2015.06.002>
48. ASTM ASTM E1820 (2022) -21 standard test method for measurement of fracture toughness. *ASTM B Stand*
49. Green G, Knott JF (1975) Effects of side grooves on initiation and propagation of ductile fracture. *Met Technol*. <https://doi.org/10.1179/030716975803277212>

Publisher's Note Springer Nature remains neutral with regard to jurisdictional claims in published maps and institutional affiliations.